Revealing the Slow Decomposition Kinetics of Type-I clathrate $Ba_8Ga_{16}Ge_{30}$

Hazel Reardon,[a] Anders B. Blichfeld,[a†] Hidetaka Kasai,[a,b] Hao Yin,[c] Espen Drath Bøjesen[a#] and Bo. B. Iversen[a*]

Inconsistencies in high temperature thermoelectric property measurements of $Ba_8Ga_{16}Ge_{30}$ have prompted our study on the thermal stability of this heavily studied inorganic clathrate. Using X-ray diffraction, thermal analysis, and imaging techniques on both powder and spark plasma sintered pelletized samples, we probe the structure and decomposition characteristics of this important high temperature thermoelectric material. We demonstrate that the decomposition of $Ba_8Ga_{16}Ge_{30}$ is extremely dependent on the heating conditions employed and, as a result of the slow decomposition kinetics of the clathrate, reveal that the true stability of this system has been overlooked in the extensive literature available. Loss of Ga and Ge from the clathrate cage is evident in all high temperature experiments under both air and inert environments. This study serves to highlight that the underlying structural chemistry and stability of thermoelectric materials at high temperature needs to be considered in parallel with the thermoelectric properties which constitute the Figure of Merit. Only then will reliable thermoelectric modules for real applications be realized.

Introduction

High temperature thermoelectric modules require stable materials for reliable extended operation. Thermal stability should therefore be one of the most important aspects to be considered in thermoelectric materials research if thermoelectric generators (TEGs) are to be deployed for high temperature applications. In reality, however, most materials are advanced simply on the premise of obtaining a high thermoelectric Figure of Merit. The thermoelectric Figure of Merit, $zT = \frac{S^2 \cdot \sigma}{\kappa} T$, is calculated from the Seebeck coefficient (S), the electrical conductivity (σ), the thermal conductivity (κ) and the absolute temperature (T), and it scales with the conversion efficiency of a thermoelectric module. However, zT only provides an indication of the viability of the performance of a material at a specific temperature condition and is a useful predictive tool for those pursuing new systems. It does not implicitly suggest that the material itself will remain unchanged at those conditions. Therefore, robust integrity tests must be performed on prospective thermoelectric materials to examine their chemical stability. Type-I clathrates [1] have long been considered a thermally stable option for thermoelectric modules, and $Ba_8Ga_{16}Ge_{30}$ (BGG) is one of the most heavily studied clathrates for thermoelectrics, albeit predominantly at low temperature [2-4]. There are inconsistencies in the thermoelectric property measurements reported at high temperature (300-1000 K) for BGG, which covers the temperature range in which this clathrate is intended for use in TEGs.

The Seebeck coefficient data for BGG was measured up to 870 K by Kuznetsov *et al.* in 2000, and shows significant deviation from their predicted model, where the authors suggested that more than one conduction band could be influencing the measurement [5]. Similarly, the plot of resistivity *vs.* inverse temperature given in the same article also shows significant deviation from their predicted model. This was attributed to the additional scattering processes resulting from impurity ions. The outcome of that study was the suggestion that tuning the composition could lead to improved *zT*, and a plethora of studies thereafter have been focused on the synthesis and tuning of BGG for high temperature applications.

The *zT* for a Czochralski grown *n*-type $Ba_8Ga_{16}Ge_{30}$ single crystal was predicted to peak 1.63 at 1100 K by Samarat *et al.* in 2006 [6]. This value was arrived at based on extrapolation of thermoelectric property measurement data, and under the assumption that the heat capacity (c_p) was constant above 1000 K. Overall, a decrease in thermal conductivity with increasing temperature was described, but an obvious anomaly (*i.e.*, increase) in thermal conductivity over the 500-800 K range was left unexplained. Their article shows only one heating curve of the property measurements of these samples, stating that repeat measurements were consistent with those given in the article and that the BGG samples are thus highly stable. It is unclear whether these additional measurements were conducted on the same sample to identify if differences were observed after repeated cycling, and the heating conditions were not given for any of their variable temperature measurements. The resistivity data for poly- and single crystalline BGG samples prepared by Toberer *et al.* also displayed an anomaly [7]. Their resistivity data exhibited a change in the gradient at approx. 500 K, which is particularly prominent for the polycrystalline sample. This is in analogy to the data presented by Kuznetsov *et al.*, and in the same region as the unusual data characteristic observed by Samarat *et al*. In 2008, the optimization of carrier concentration in polycrystalline $Ba_8Ga_{16-x}Ge_{30+x}$ intended for use at high temperatures was investigated by Martin *et al.* by small variations in cage composition; $0.5 \leq x \leq 1.2$ [8]. They describe metallic-like resistivity behavior for all samples with varying

[a] *Center for Materials Crystallography, Department of Chemistry and iNANO, Langelandsgade 140, Aarhus University, 8000 Aarhus, Denmark.*
[b] *Faculty of Pure and Applied Sciences, Center for Integrated Research in Fundamental Science and Engineering, and Tsukuba Research Center for Interdisciplinary Materials Science, University of Tsukuba, 1-1-1 Tennodai, Tsukuba, Ibaraki, 305-8571, Japan*
[c] *TEGnology, Lundagervej 102, 8722 Hedensted, Denmark.*
† ABB is currently at the Department of Materials and Engineering, Norwegian University of Science and Technology (NTNU), NO-7491, Trondheim, Norway.
# EDB is currently at the Monash Centre for Electron Microscopy, Monash University, Innovation Walk 10, 3168 Clayton, VIC, Australia.
Electronic Supplementary Information (ESI) available: . See DOI: 10.1039/x0xx00000x

Ga:Ge contents, but closer inspection of these data plots clearly demonstrate non-linear behavior. Between 200-300 °C, an increase in gradient for a number of the resistivity plots is observed. Since an increase in resistivity is associated with a decrease in charge carrier concentration, it is possible to suggest that the decrease in charge carrier concentration is related to variation of the Ga:Ge ratio in the clathrate cage. The *zT* plots given by Martin *et al*., clearly show two distinct gradient regions, which intersect at approximately 400 °C, with the gradient at higher temperatures being more positive than the lower temperature region. May *et al.* also recorded the thermoelectric properties of polycrystalline *n*- and *p*-type $Ba_{8.2}Ga_{16-x}Ge_{30+x}$ (x = 0.76, 0.50, 0.47,0.10, -0.18) revealing an unusual characteristic in the heat capacity measurements at 650 K for both x = 0.50 and -0.18 [9]. The thermal diffusivity of the samples was determined to decrease with decreasing carrier concentration, with the most prominent drop observed for the sample with the lowest Ga:Ge ratio: 0.49 (*vs.* 0.533 for the nominal stoichiometry).

In contrast to the studies described so far, which focus on a very narrow Ga:Ge cage composition range, Okamoto *et al.* recorded the structure and property modifications of $Ba_8Ga_xGe_{46-x}$ (x = 3-18) [10]. They demonstrated that a Type-I superstructure analogous to $Ba_8Ge_{43}\square_3$ ($Ia\bar{3}d$) is evident when x = 3.5-5. From synchrotron powder X-ray diffraction data, they observe that there is a proportional relationship between Ga content in the Type-I clathrate (x =3-16) and the elemental α-Ge impurity phase observed in all samples; with increasing Ga, the α-Ge impurity decreases. This conclusion was corroborated by Rietveld refinement of the Ge vacancies in the cage structure, where the number of vacancies also decreased as a function of increasing Ga. Through their property measurements, they showed that the superstructure samples (*i.e.*, those with sub-stoichiometric cage composition) possess higher resistivity at 50 °C than the samples which are described by the regular Type-I lattice ($Pm\bar{3}n$). This article thus confirms that the Ga: Ge ratio is important for stabilizing the clathrate cage in the Type-I structure, and that both the physical and chemical properties of the clathrate are affected by changes to the cage composition. Moreover, the change in resistivity as a result of varying Ga:Ge ratio could provide a more robust explanation for the unusual property results at high temperature presented elsewhere.

Regarding studies which focus specifically on the stability of BGG, Cederkrantz *et al.* found that Ga evolved upon heating *p*-type $Ba_8Ga_{16}Ge_{30}$ prepared by the Ga flux method [11]. They describe that a 10 % mass loss is evident in p-type samples as a result of heat treatment *in vacuo*, and that heat treatment at 600 °C results in a flip in carrier type from *p*- to *n*-type, although this was not observed in the samples heat treated at 400 °C or 800 °C. They suggest that this arises from a complex relationship between the kinetics and thermodynamics of Ga loss, but no robust thermal analysis methods were used in their study to identify the thermal profile of the samples as they were heated. In addition, they state that their diffraction results identified the clathrate to remain as the Type-I structure even after annealing, but did not demonstrate or discuss any of their diffraction data further. This is unusual, since such a significant change in the cage composition by loss of Ga would have been evident from, for example, a change in relative intensity of the reflections or as a shift in the reflection positions, corresponding to a change in the unit cell parameter. Furthermore, the stability was only tested using one heating rate and none of the samples were cycled. Therefore, a complete overview of the stability of BGG is yet to be realized.

In spite of this, Köhler *et al.* used n-BGG in a high temperature thermoelectric generator (TEG) module [12]. Remarkably, this study demonstrated that the TEG was functional up to 800 °C and that the module operation was not hindered upon exposure to a thermal gradient up to 123 °C. Despite these promising results and from the information provided, no consideration was given to the effect of heating on the structure or composition of the material itself after heating or thermal gradient exposure. Based on the relatively few data points and the short measurement times used in this recent study, it is unlikely that any kinetic effects could be observed within the 3 h period employed. Therefore, the success of this study should be considered only for the timescales employed therein, where extrapolation of data to justify stability over longer time periods is likely to be unreliable.

A thorough investigation of the correlation between the BGG structure and properties as a function of elevated temperature does not yet exist. From existing literature we know that the BGG unit cell is described by the cubic space group $Pm\bar{3}n$ (No. 223); dodecahedron and tetrakaidecahedron host cages comprised of Ga and Ge enclose the Ba guest atoms (SI.1).

There is a clear gap in the understanding of high temperature characteristics of BGG. The purpose of this study, therefore, is to investigate and define the thermal stability of $Ba_8Ga_{16}Ge_{30}$ under a variety of high temperature configurations with a focus on the underlying chemistry of the clathrate. Not only is this useful for developing our understanding of clathrates generally, but it will enable a deeper understanding of the inconsistencies observed for BGG in previous high temperature studies. Ultimately, this will establish the temperature conditions in which the clathrate is stable and whether this candidate material is truly suitable for high temperature TEG modules. It will serve as an example for how fundamental studies on high temperature properties of materials should be investigated (in synergy with property measurements). Herein, a multi-technique approach has been employed, combining techniques that have not yet been previously assimilated to describe this system. Using data obtained from samples prepared by carefully considered annealing experiments and calorimetry, conventional laboratory and variable temperature synchrotron X-ray diffraction, and electron microscopy and diffraction, we are able to draw conclusions about the property-structure relationships of both polycrystalline powder and dense bulk BGG clathrate samples at high temperature from a completely unique perspective.

Experimental

Sample Preparation and Heat Treatment

Polycrystalline $Ba_8Ga_{16}Ge_{30}$ was prepared by a standard melt synthesis method, where the elements were melted in a glassy carbon crucible *in vacuo*. All materials handling was conducted in a glovebox to prevent oxidation. Lustrous pieces of Ba were cut from a rod (Sigma Aldrich, ≥99% trace metals basis), Ga shot (Alfa Aesar, 99.99% trace metals basis) was gently heated to above room temperature to remove impurities from the melt before use, and Ge lump (Alfa Aesar, 99.9999 %) was crushed to a fine powder in a glovebox before use to minimize surface oxidation. A slight excess (5 wt%) of Ba was employed to circumvent losses due to evaporation. The elements were added to the crucible then heated at 200 °C/h to 1050 °C and held for 6 h, before cooling in a controlled stepwise manner; 1) 75 °C/h to 950 °C with 2 h dwell, 2) 5 °C/h to 850 °C with 0.5 h dwell, 3) 100 °C/h to 700 °C with 48 h dwell, followed by furnace cooling to room temperature. The resultant ingot was crushed to a powder in a mortar and pestle before washing in 4 M $HCl_{(aq)}$ for 24 h to remove any acid soluble impurities, *i.e.*, residual Ba. The acid-washed powder was then subject to an iterative washing process in ethanol and water until the washings were pH neutral. Finally, the washed dark grey powder was allowed to dry in air. Powder from the same clathrate sample batch was subject to a number of annealing experiments (Table 1), using 0.5 g of the BGG powder per annealing experiment. The samples were weighed into alumina crucibles and annealed under air in a box furnace between 300-730 °C. For comparison, a sample was also annealed at 730 °C in a carbon coated fused silica crucible *in vacuo*.

Thermal Analysis

Thermogravimetric-Differential Thermal Analysis (TG-DTA) and Thermogravimetric-Differential Scanning Calorimetry (TG-DSC) were used to compare the thermal profile of the annealed samples with that of the baseline clathrate which had not been heat treated post-synthesis. All thermal analysis was performed on a Netzsch STA (Simultaneous Thermal Analysis) 449C Jupiter instrument. Calibration of the instrument was conducted using seven melting point standards: In, Sn, Bi, Zn, Al, Ag, Au.

Table 1. List of annealing conditions used in this study, where the annealing temperature (in °C) is indicated in the sample name.

Sample ID	Anneal Duration
1_MS	No anneal
2_MS_300a	96 h
3_MS_400a	96 h
4_MS_500a	96 h
5_MS_600a	96 h
6_MS_730a	96 h
7_MS_730v	96 h
8_MS_SPS	SPS anneal
9_MS_SPScyc	100 cycles
10_MS_SPSsus	6 days

(MS = Melt Synthesis, SPS = Spark Plasma Sintering, a = air, v = vacuum, cyc = cycled thermal gradient, sus = sustained thermal gradient.)

These standards cover the entire temperature range employed in this work (temperature resolution = 0.001 K; balance resolution = 0.025 μg). Measurements were performed under $Ar_{(g)}$ (flow rates: purge gas = 50 mL/min, protective gas = 40 mL/min) with a heating rate of 10 K/min for the TG-DTA measurements, where both the heating and cooling profiles of the samples were collected. Furthermore, a number of cycling experiments below and above the melting point of the clathrate were performed by TG-DTA to examine the impact on the thermal profiles of the samples after repeated heating experiments. For DSC measurements, correction files were collected for each heating rate; 2, 5, 10 and 20 K/min, then sample-plus-correction measurements were performed (DSC enthalpy accuracy = ±2 %). The residues in the alumina pan were collected after each thermal analysis measurement to examine the product remaining after heating. The Proteus® software provided by Netzsch was employed to examine the data. The extrapolated onset temperature was used for the melting point features since the peak temperature is mass dependent, although the peak temperatures are also given here for completeness.

Spark Plasma Sintering

An SPS-515 instrument (SPS SYNTEX INC, Japan) was used to prepare dense pellets of the clathrate. The powdered sample was contained in a high density graphite ½" die, the inner surfaces of which had been coated in a fine layer of commercial BN spray. The circular ends of the punches that were in contact with the sample were also coated in BN, but the outer surfaces of the punches in contact with the die were coated with graphite paper. The optimum sintering profile was then determined by an iterative process. The following SPS conditions were employed thereafter: the chamber was evacuated, the pressure was preset to 100 MPa and then a temperature applied at a 100 °C/min ramp rate to 800 °C followed by 5 min dwell at these conditions. The pressure was subsequently released over a period of 1 min and the temperature allowed to return to room temperature by natural cooling. The sample was then polished using fine sandpaper on a polishing turntable until all surfaces of the sample were free of any graphite or BN residues leftover from the sintering process. Using the optimized pressing conditions, densities of pellets prepared using these conditions were determined by the Archimedes method. The calculated densities were found to be consistent and very close to the expected value of 5.85 g/cm^3. The density of the pellet used for the thermal gradient test was 5.82 g/cm^3.

Thermal Gradient Testing

The SPS sample was broken in to a number of smaller fragments and subject to two different thermal gradient tests; sustained (sus) thermal gradient and cycled (cyc) thermal gradient, using a bespoke furnace-cooler set-up in air. The assembly employed a heater on the bottom surface of the sample, which was controlled by a Eurotherm temperature controller, and a heat sink on the upper surface for cooling. Graphite paper was

placed on both upper and lower surfaces of the pellet pieces to improve heat conduction and eliminate any possibility of contamination from the furnace. The hot and cold sides were approximately 400 °C and 50 °C respectively, giving a thermal gradient of ca. 350 °C. The sustained thermal gradient involved maintaining the thermal gradient across the pellet constantly. For the cycled thermal gradient, the heater was programmed to repeatedly cycle the hot side up to 400 °C and then back to room temperature. This was conducted for 100 heating and cooling cycles. Images of the pellets were collected immediately after the thermal gradient test using an optical microscope.

X-Ray Diffraction and Rietveld Refinement

Conventional laboratory powder X-ray diffraction (PXRD) was conducted on both powders (as-prepared and annealed) and bulk SPS treated samples using a monochromatic Cu-$K\alpha_1$ X-ray source (λ = 1.54056 Å). In addition, some of the samples were investigated at the SPring-8 synchrotron facility (BL44B2, Riken, Japan) at both room and high temperature (hereafter described as SXRD). The beam sizes employed for the room and high temperature configurations were 0.5 × 3 mm and 0.5 × 1 mm, respectively.

To ensure a good powder average for the measurements, the smallest crystallites of the powders were selected by a floating method involving dispersion of the samples in an appropriate solvent, *i.e.*, ethanol. The fine powders were then dried and packed as densely as possible in to 0.2 mm glass or quartz capillaries (for room temperature and high temperature measurements, respectively) in air. The high temperature measurements were conducted between 300 K - 1000 K, employing a heating rate of 50 K/min and measurement intervals of 100 K after a 120 s thermal equilibration period at each temperature. After heating, the same sample was re-measured upon return to 300 K in order to verify any modifications to the sample before and after heating.

The Rietveld method was used to compare and refine the data with a suitable structure model where possible in order to elucidate relevant structure characteristics and modifications with respect to temperature. The MAUD software was used to perform the Rietveld refinements in this study [13]. The instrument resolution was determined using the diffraction data collected on a NIST 674b CeO_2 standard to account for the instrumental contributions to the data. The CeO_2 standard data was also used to extract the exact wavelength used. Parameters used for refinement of the clathrate data included background contribution, unit cell parameters, all general atomic postions (for simplicity, we assume Ba2 lies in the centre of the cage, *i.e.*, the high symmetry 6*d* Wyckoff site), and isotropic B_{iso} values were refined for Ba1 and the cage atoms. For Ba2, anisotropic B_{aniso} values were refined. Full occupancy of the guest and cage atoms was assumed, with random distribution of Ga and Ge on the three framework positions, per the values given in reference 14.

TEM-EDS

A metallic globule obtained from 9_MS_SPScyc after the thermal gradient cycle test was crushed finely in a small amount of ethanol using an agate mortar and pestle that had been thoroughly cleaned, which was important to avoid contamination of the specimen. The ethanol dispersion was then carefully deposited dropwise on to a carbon coated copper TEM grid. Spatially resolved elemental analysis, with a spatial resolution better than 2 nm, was obtained using a TALOS F200A microscope in STEM mode and equipped with a Super-X EDS Detector. Exposure times of 7 minutes were used to create elemental distribution maps with satisfactory counting statistics. Data was collected and visualized using the Bruker Esprit software.

SEM-EDX

SEM-EDX (Scanning Electron Microscopy-Energy Dispersive X-Ray spectroscopy; FEI Nova 600 Nano SEM, TLD detector in secondary electron mode under high vacuum) allowed quantitative analysis of Ba, Ga and Ge on the hot and cold surfaces of 9_MS_SPScyc and 10_MS_SPSsus, respectively. Three distinct areas (1.52 mm^2) on the surface of each of the samples were measured, to indicate (in-)homogeneity and allow an average composition to be derived for each of the surfaces.

Results

Baseline Structure and Thermal Properties

PXRD data for 1_MS were collected at SPring-8, and exhibited the characteristic diffraction reflections for the Type-I clathrate. Rietveld analysis gives a sensible fit to the structure model previously given by Bentien *et al*. (SI.1) [14]. The DTA profile of 1_MS exhibits two endothermic features (Figure 1); the first at ca. 772 °C, and the second is attributed to the melting of the clathrate, at 982.2 °C. (Comparison with duplicate BGG samples prepared in the same way revealed similar high temperature features.) Previously reported values (957±5 [15], 967 [16] and 974±5 [5] °C), have shown reasonable variability in the melting point, but no mention of this lower temperature feature is evident in the literature. No mass loss was observed throughout the TG-DTA experiment, indicating that no evaporation occurred.

The PXRD and TG-DTA data for MS_1 are considered the 'baseline' diffraction data and thermal profile for this study, i.e., data collected on the annealed samples are compared to these data and deviations allow comparisons to be made across the sample series. It is important to note that the annealed powder samples were all derived from the same BGG sample batch (1_MS), to ensure absolute comparison between the baseline and annealed samples.

Annealed Powder Samples

Visual Observations

After annealing batches of 1_MS at different temperatures in air/vacuum, some obvious changes visible by eye were noted; 3_MS_400a appeared deep blue relative to the original dark

grey BGG clathrate powder, but this was not the case for 2_MS_300a, 4_MS_500a or 5_MS_600a, which only became slightly darker. Sample 6_MS_730a was significantly paler than the other samples, suggesting a significant change of the sample. In contrast, 7_MS_730v remained a dark grey powder after annealing.

PXRD

The characteristic Bragg peaks for Type-I BGG were evident in the PXRD patterns of all of the annealed powder samples measured at room temperature. The intensity of the reflections attributable to the α-Ge phase increases significantly between sample 3_MS_400a and 4_MS_500a, and again between 4_MS_500a and 5_MS_600a (Figure 2). Annealing at 500 °C (4_MS_500a) appears to cause the formation of reflections which may be attributed to a supercell (Figure 2 Inset), suggesting ordered vacancies in the cage of the Type-I structure; analogous to $Ba_8Ge_{43}\square_3$ [17].

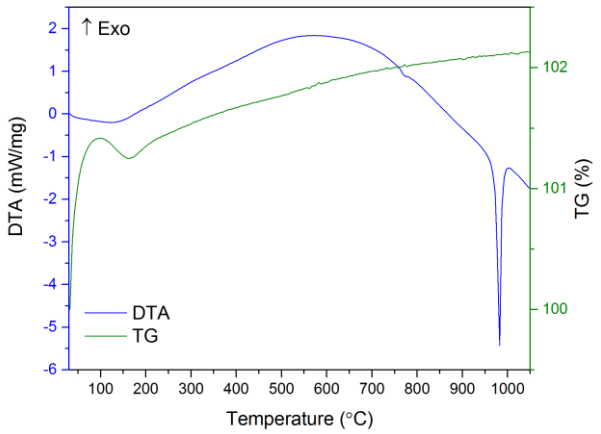

Figure 1 – TG-DTA heating profile of 53.660 mg of 1_MS.

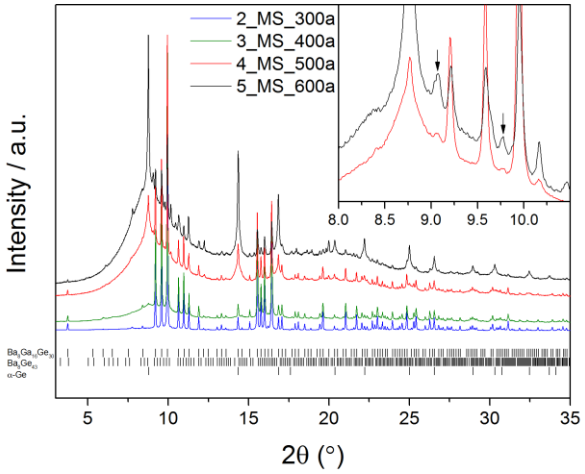

Figure 2 – Comparison of normalized PXRD patterns for 2_MS_300a to 5_MS_600a collected at 300 K using λ = 0.500304(7) nm. The inset shows a low order diffraction pattern region of 4_MS_500a and 5_MS_600a, where downward arrows indicate the supercell reflections. Upper, middle and lower tick marks are for Type-I BGG, supercell structure Ba_8Ge_{43} and α-Ge, respectively.

Focusing on the 8-10° region of 4_MS_500a PXRD data, there appears to be two reflections at 9.1°, which become more disparate in the diffraction pattern of 5_MS_600a. The lower intensity, low angle peak can be assigned to the supercell and the other peak at a slightly higher angle could reveal the formation of the *c*P124-Type Ba_6Ge_{25} phase [18]. Furthermore, it is obvious that an amorphous component of the sample develops as the annealing temperature is increased. This is evidenced by the elevated background feature in the diffraction patterns in the low angle region between 2θ = 5-14°, and can most likely be attributed to the evolution of $Ga_{(l)}$. The supercell reflections in the 2θ = 3-9° region that were identified in BGG previously by Okamoto *et al.*[10] are likely to be obscured by the amorphous component which arises in this work.

Using the MAUD software, the room temperature data collected for the annealed samples 2_MS_300a to 5_MS_600a were refined using the Rietveld method (SI.2). The same refinement parameters that were used for the baseline refinement for 1_MS were employed, where the background was adjusted manually to account for the amorphous component in the annealed samples. In all annealed powder samples, the unit cell parameter of BGG is decreased relative to 1_MS, indicating a contraction of the lattice after annealing. The shrinkage of the lattice is consistent with a reduction in size of the clathrate cages, which is likely to be caused by the loss of Ga and Ge. It is important to note that the unit cell decreases in sample 3_MS_400a relative to sample 2_MS_300a, but then increases again in sample 4_MS_500a. Thus, sample 4_MS_500a may be interpreted as an outlier, since the unit cell of sample 5_MS_600a decreases linearly with respect to samples 2_MS_300a and 3_MS_400a. This anomaly in the unit cell of sample 4_MS_500a can be explained considering that the formation and crystallization of the supercell is likely to modify the lattice. Here this appears to be manifested as a slight expansion of the unit cell. The proportion of Ge (relative to BGG) was also determined, which was <1% in 1_MS and remained so until 4_MS_500a, whereupon the phase fraction of Ge increased dramatically to 40.2(2)%, and to 56.6(5)% in 5_MS_600a.

The diffraction data for sample 6_MS_730a show that the sample is multiphase and that the clathrate has almost completely decomposed, with only very low intensity reflections evident from the Type-I clathrate phase. It has not yet been possible to identify all of the phases in this samples, and so Rietveld refinement of this data was not performed for inclusion in this study. Variable temperature synchrotron X-ray diffraction shows that sample 6_MS_730a does not appear to decompose further up to 1000 K during the variable temperature synchrotron experiment (SI.3). A more thorough analysis of the variable temperature synchrotron PXRD data will be presented in a separate article.

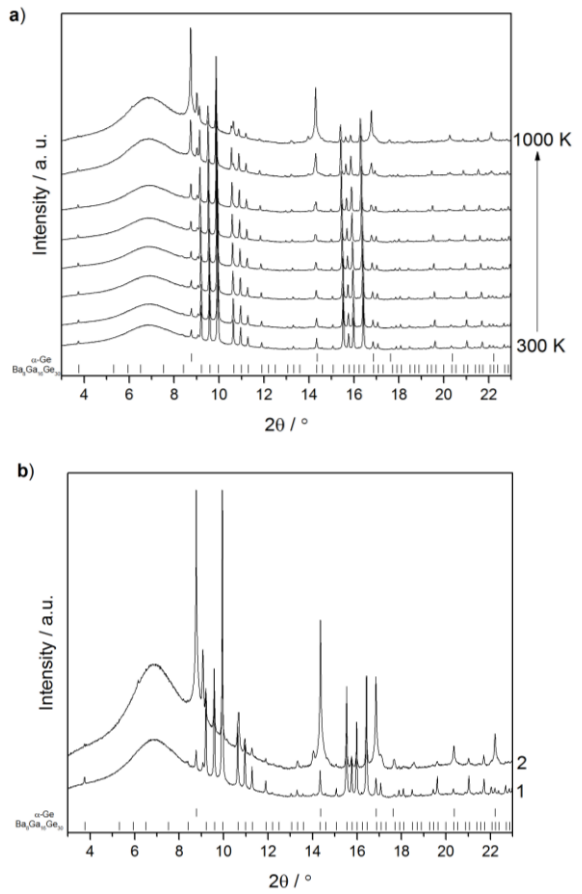

Figure 3 – a) Normalized variable temperature PXRD data for 4_MS_500a collected in the 300-1000 K temperature range. b) Comparison of the 300 K data collected before (1) and after (2) heating. (Upper and lower tick marks indicate α-Ge and Type-I clathrate reflections, respectively.)

From the room temperature PXRD data collected for 2_MS_300a through to 5_MS_600a, all of the samples appear to undergo similar phase modifications; the modifications are enhanced at higher annealing tempera-tures.Therefore, variable temperature SXRD was employed for 4_MS_500a in an attempt to monitor if the decomposition developed further. This experiment revealed a number of interesting features (Figure 3a). As previously noted, the α-Ge phase is present at 300 K, but the intensity of the α-Ge reflections are enhanced in the 800 K dataset relative to the 300-700 K data. In the 800 K dataset, the impurity reflection at ca. 9° becomes more intense and in the 1000 K data the intensity of the reflections from the main BGG phase are significantly diminished relative to the 300 K data. This suggests that the sample undergoes a significant change upon heating in air between 700 K and 800 K at a heating rate of 50 K/min. Comparison of the data collected before and after heating, given in Figure 3b, reveals the stark difference in the samples, where there is an increase in the intensity of the amorphous feature, and the reflections for α-Ge and the unknown phase are prominent. The room temperature dataset of 7_MS_730v revealed the same signs of decomposition as the air annealed samples (SI.4); given by the presence of the more intense α-Ge reflections (relative to the as-prepared material) and the reflection at 9.1° from the unknown phase. A variable temperature diffraction study was also performed on this sample, which shows that it will continue to decompose upon further exposure to high temperatures (Figure 4). In analogy to 4_MS_500a, the data plots given in Figure 4a clearly show that the α-Ge and impurity phases develop further at 800 K, highlighting that a change has taken place between 700 K and 800 K. The sample was subject to two thermal cycles to 1000 K at the synchrotron to determine if the decomposition was enhanced after two cycles. The 2nd cycle did not include intermediate temperature measurement steps as in the first cycle, therefore we expect the thermal exposure to be somewhat different to the first cycle, i.e., a shorter heating duration. The data collected at 300 K are shown in Figure 4 b, where the 2nd cycle does not seem to have significantly affected the phase composition of the sample; and this is likely to be a result of the shorter exposure time of the sample to the high temperature. This highlights that the decomposition of BGG is strongly influenced by kinetics: shorter thermal exposure time, less decomposition and *vice versa*. The two datasets collected at 1000 K are given in SI.5 and very closely resemble one another. Due to the limited time available at the synchrotron, it was not possible to determine if the decomposition was exacerbated after two heating cycles under the same conditions. It is interesting to note, however, that the same decomposition features were observed in both the air and vacuum annealed powders.

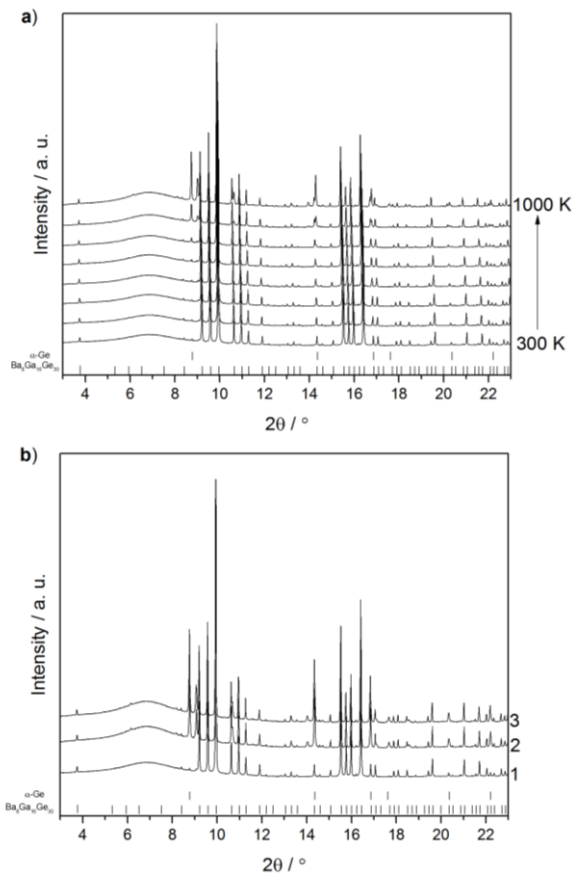

Figure 4 – a) SXRD patterns of sample 7_MS_730v from 300 K – 1000 K. b) PXRD data collected at 300 K before heating (1) and after 1st (2) and 2nd (3) heating to 1000 K. (Upper and lower tick marks represent the reflection positions for the α-Ge and Type-I clathrate reflection positions, respectively.)

Thermal Analysis and STA Cycling Experiments

The DTA traces of the air annealed samples demonstrate that the thermal profile of BGG is significantly affected after annealing in air and more so at higher annealing temperatures (Figure 5, Table 2). Close inspection of the DTA data, however, reveals that the onset of the melting point of the clathrate decreases as the annealing temperature is increased from 300 °C to 400 °C, i.e., from 2_MS_300a to 3_MS_400a. An extremely broad peak profile is observed in 4_MS_500a over the region in which one would expect the melting of the clathrate phase.

This re-emergence of a distinct melting feature suggests that a phase which is dissimilar to the clathrate has formed.The TG-DTA data for sample 6_MS_730a (Figure 5b)) agree with the observations from variable temperature PXRD data (SI.3), showing no additional decomposition features in the 300-1000 K range. Figure 5b shows that above approx. 1000 K, however, there is a major endothermic decomposition event associated with significant mass loss of >20 % *via* a number of decomposition steps. It is unclear what this mass loss is attributable to with the data available, and since the sample appears to be multiphase it could be the simultaneous decomposition of a number of components in the sample. Sample 7_MS_730v showed that the vacuum annealing had a very small effect on the thermal profile of the clathrate, relative to the air annealed samples (SI.6). The area of the BGG melting curves was determined where possible, which decreases as the annealing temperature is increased. The area of the clathrate melting curve could not be determined for samples 5_MS_600a and 6_MS_730a, because this feature was not evident or extremely broad and thus considered indistinguishable in the corresponding DTA data. The diminished melting feature reflects the diminishing proportion of the original BGG clathrate remaining after the annealing experiments, but the percentage of is somewhat lower than that obtained from Rietveld refinement of the PXRD data. This may be because of the broadening of the DTA features, which indicates that the sample is melting over a broader temperature range. This, in turn, may indicate a wider composition range for BGG than was employed in the refinements, suggesting an overestimation of the original BGG phase in the refinement. A splitting of the lower temperature feature and a lowering of the onset melting temperature is clear from the DTA plots in Figure 5. The splitting feature reveals an exothermic event followed by an endothermic event, where the former suggests the crystallization of a new phase, and may be assigned to the formation of the supercell structure which possesses vacancies or the realization of a range of cage compositions.

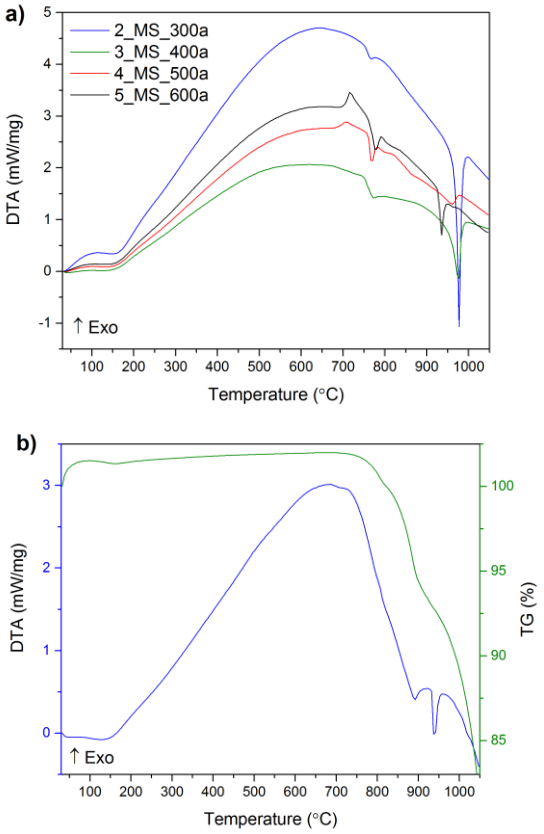

Figure 5 - a) The corresponding DTA traces for samples 2_MS_300a-5_MS_600a and b) TG-DTA profile for sample 6_MS_730a.

Table 2. Data derived from DTA measurements.

Sample	Onset (°C)	Melting Point (°C)	Peak Area (J/g)	Area Comparison (%) [($Area_{1\_MS}/Area_{anneal}$)*100]
1_MS	973.2	982.2	-281.6±5.6	-
2_MS_300a	968.8	977.7	-249.2±5.0	88.5
3_MS_400a	961.3	975.5	-194.8±3.9	69.2
4_MS_500a	925.0	961.6	-43.75±0.9	15.53
5_MS_600a	928.3	935.1	-46.81±0.9	-
6_MS_730a	932.8	939.4	-37.31±0.8	-
7_MS_730v	971.5	979.6	-263.3±5.3	93.5
8_MS_SPS	971.2	982.5	-264.5±5.3	93.9

This corresponds well with the PXRD data, since a surplus of α-Ge develops together with evolution of Ga melt (*i.e.*, the amorphous component), which would both result in vacancy formation. The latter event at 770 °C may be attributed to the melting of the supercell clathrate. Indeed the melting of $Ba_8Ge_{43}\square_3$ is reported to occur at approximately 814 °C [19]. The melting point of the feature at 770 °C increases as the annealing temperature increases from 500 °C to 600 °C, suggesting that more of the sample has been converted to the new off-stoichiometry phase. Combining the PXRD and DTA results, a range of BGG compositions is likely to exist as a result of the Ga and α-Ge losses arising from high temperature treatment.

A number of TG-DTA experiments at 10 K/min under $Ar_{(g)}$ flow were conducted on sample 1_MS to elucidate information about how the thermal profile of the sample changes over repeated heating cycles both below and above the melting point (Table 3). Despite intended applications having working temperature below the melting point of BGG, inclusion of the melting feature is important to determine resultant changes in the melting profile of the clathrate. This reveals information about how the sample has been modified relative to the original, un-annealed clathrate sample (**A**, Figure 1b). The disparity between 1st and 2nd heating profiles in regime **B** (Figure 6a) reveal that the enthalpy (derived from the area under the curve) associated with the melting curve of the clathrate was diminished in the second heating relative to the first (-278.3±5.6 *vs.* -225.8±4.6 J/g). The minor endothermic feature at 770 °C became a broad feature spanning from 650-900 °C after the first melt. The thermal profile of the melting feature in regime **C** is distinct from **A** (Figure 6b), where the lower temperature feature is more enhanced and the area of the melting curve is significantly diminished. From this, we know that heating the sample repeatedly to 730 °C, even in $Ar_{(g)}$, causes the clathrate to decompose. Despite the very small quantity of sample, laboratory PXRD data were collected after A, B and C, where all data showed that the sample retained a phase with the Type-I clathrate structure, with no evidence of the supercell reflections. In all samples, the α-Ge reflection was more intense relative to 1_MS, and additional reflections from the same impurity phases found in the annealed samples were evident.

The (222) and (321) reflections of the Type-I phase exhibit a shoulder to the low angle side of the reflection, while a more resolved reflection on the low angle side of (320) is clear. One could speculate that a second clathrate phase with a smaller unit cell has been formed, but was not visible (or was overlooked) within the heating conditions in which BGG has previously been studied. Since the PXRD data reveals that a proportion of the BGG phase remains, even after a number of TG-DTA heating cycles, this data provides further evidence that the decomposition kinetics are very slow. To corroborate this, TG-DSC measurements on **1** were performed using a variety of heating rates. It is obvious from the data shown in Figure 6c that the thermal profile of the sample is significantly influenced by the heating rate, where the melting feature of the Type-I clathrate is virtually non-existent in the 2 and 5 K/min experiments, and the enthalpy associated with the melt determined from the area under the curve is diminished between 20 and 10 K/min (-129.4±2.6 and -103.4±2.1 J/g respectively). The low temperature feature at ca. 770 °C remains throughout each of the heating rate experiments.

Table 3. Series of TG-DTA experiments examining the effect of heating and heating cycles on sample 1_MS. (*Data shown in Figure 1.)

TG-DTA Experiment ID	Heating Profile (°C)	Extrapolated Onset (°C)		Melting Point (°C)	Curve Area (J/g)
A*	RT→1050→RT	-			
B	RT→1050→RT→1050→RT	Peak 1	Cycle 1: 775.6	770.8	-3.9±0.1
		Peak 2	Cycle 1: 970.5	983.6	-278.3±5.6
			Cycle 2: 964.5	979.4	-225.8±4.6
C	RT→(730→RT)×5→1050→RT	Peak 1	759.7	772.7	-50.8±1.0
		Peak 2	964.6	977.5	-162.2±3.2
D	RT→(730→RT)×5	-			

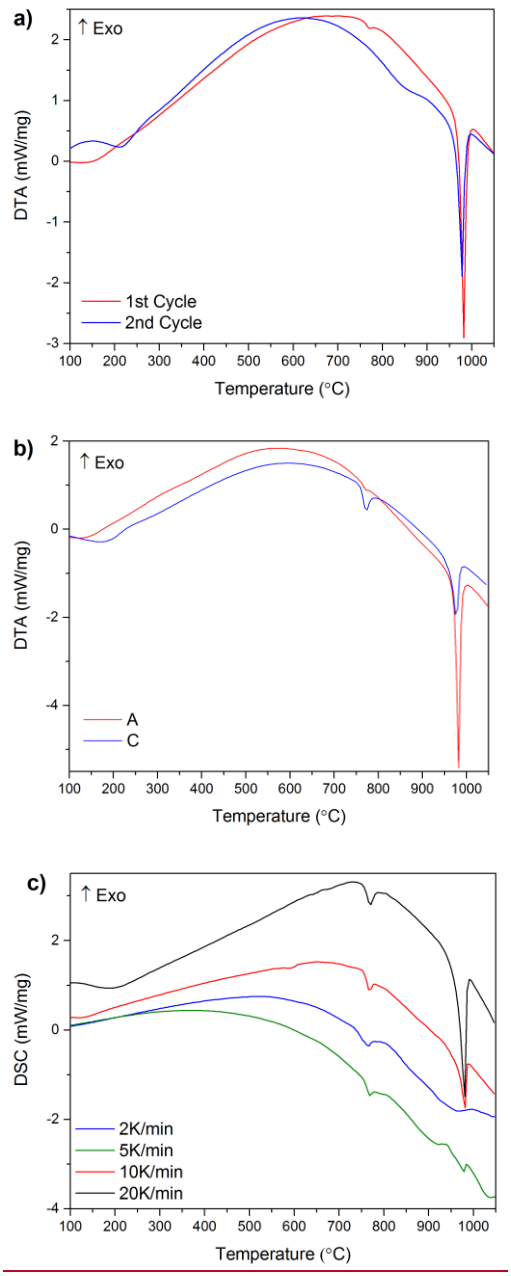

Figure 6. a) DTA heating traces for experiment **B**, and b) DTA traces of experiments **A** and **C** comparing the stark difference in the melting curves obtained. c) DSC data for 1_MS collected at various heating rates.

SPS Pressing

The SPS pellet was divided in to a number of pieces; one piece was ground to a fine powder (8_SPS), and the remaining pieces were used for the thermal gradient tests described below (given as samples 9_MS_SPScyc and 10_MS_SPSsus in Table 1). Sample 8_SPS was examined by both PXRD and TG-DTA. The diffraction pattern (given in SI.7) resembles that of 1_MS (SI.1). The DTA profile for 8_SPS is very similar to that of 7_MS_730v, suggesting that the thermal profile of the clathrate has only been slightly affected by SPS treatment, and is comparable to the vacuum annealed sample. This makes sense given that the SPS treatment was conducted under vacuum, although it may also suggest that the rapid SPS heating (*i.e.*, Joule heating) is almost equivalent to four days of annealing (by convective heating).

Stability In a Thermal Gradient

To compare the decomposition of powder *vs.* bulk BGG, fractions of the same SPS pressed pellet were used for thermal gradient tests (hot and cold side approximately 400 and 50 °C, respectively), using two different test conditions, cycling 100 times (cyc) or sustained for 6 days (sus). In addition, more than one fraction of the pellet was examined under the gradient simultaneously, to demonstrate if the same effect is seen on different sections of the same sample.

Thermal Gradient Cycling

Metallic protrusions on the surfaces of the pellet pieces were visible by eye upon removal from the furnace, where the sample evolved these protrusions on both the rough and smooth surfaces of the pellet (Figure 7). PXRD analysis of the 'hot' and 'cold' surfaces of the pellet was conducted after thermal cycling (SI.8a). This diffraction data revealed that the cold side was not modified significantly, but that the hot side exhibited signs of degradation; α-Ge reflections and an unknown phase.

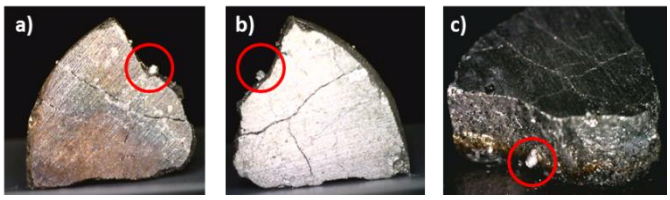

Figure 7. Images of the a) hot side b) cold side and c) rough edge of 9_MS_SPScyc showing a significant protrusion from the surface highlighted by the red circle.

It is prudent to note that the same unknown phase that was observed in the powder sample is also visible in the data for the hot side of the bulk pellet. Attempts were made to analyze the protrusions by PXRD, but the sample size was too small. TEM images/micrographs showed distinct spherical features from the dispersion of the crushed protrusion specimen, which were determined to be Ga by EDS, Figure 8, SI.9. This is somewhat surprising since we do not see any reflections from metallic Ga in the average PXRD data for the pellet nor in the powder data collected for the annealed powder samples. This reinforces, however, that the amorphous component in the SXRD data is most likely to be from liquid Ga. (It should be noted that the Si and O observed in the spectrum are from the grid, and not from the sample itself, see SI.9.)

Sustained Thermal Gradient

As in the cycling experiment, the sample exposed to a sustained thermal gradient (10_MS_SPSsus) was shown to have metallic protrusions on both the rough and smooth surfaces of the pellet, Figure 9. The PXRD analysis confirms that the hot side is significantly more affected by the thermal exposure (which is comparable to the cycling experiment), and also reveals the

same diffraction reflections observed for the powder samples upon decomposition (SI.8b).

The atom% of Ba (L_α), Ga (K_α) and Ge (K_α) determined by SEM-EDX allowed determination of the Ga: Ge ratio with respect to the hot and cold sides of the pellets (Table 4). This analysis revealed that the Ga: Ge ratio in sample 10_MS_SPSsus is more affected than in 9_MS_SPScyc, since the Ga: Ge ratio of the hot and cold sides of the former are different (while the ratio in the latter remains the same). This result confirms that the hot side is more affected than the cold side, and that the sustained gradient has a greater effect on the migration of Ga through the samples than the cycled thermal gradient.

This latter concept confirms that the kinetics of Ga (and Ge) migration is of significant importance in this system. Since many of the previous studies will have used heating cycles to investigate samples at high temperatures, the kinetics of the Ga/Ge migration is likely to have been overlooked on the timescales employed and on the typically limited number of thermal cycling experiments performed.

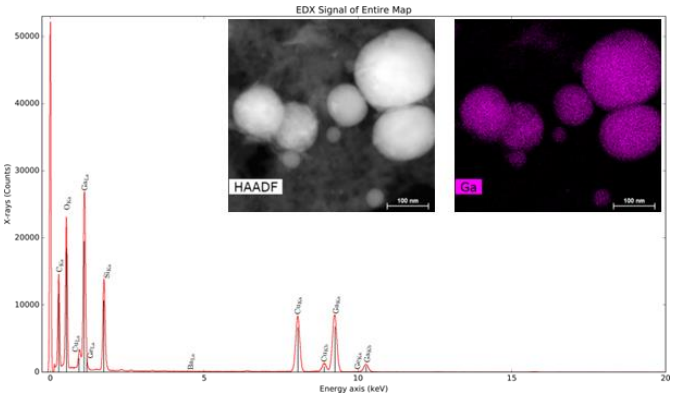

Figure 8. EDS spectrum of the sample region shown in the HAADF image given inset, and the Ga map of the same region also inset.

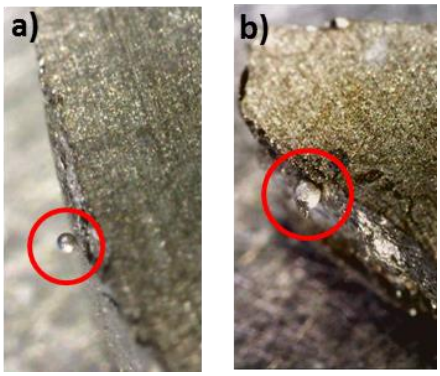

Figure 9. Images of the metallic protrusions highlighted by red circles on the a) smooth and b) rough surfaces of sample 10_MS_SPSsus.

Discussion

It is clear from the results presented here that BGG is not stable up to 730 °C, i.e., a temperature below the melting point and within the range in which it was previously reported to be stable. The decomposition products obtained after air and vacuum annealing appear to be the same based on comparison of the reflections obtained by PXRD. The decomposition kinetics under vacuum are slower than that of the air annealed samples, highlighting that the kinetics are key to observing and understanding the decomposition of this system. Diffraction data highlight that the structural changes in this clathrate are subtle, and cannot be easily observed in data collected using a conventional laboratory diffractometer. Focusing on the decomposition products observed in the diffraction data, not only do we observe an obvious increase in relative intensity of α-Ge reflections as the annealing temperature is increased, but we also see an unknown phase and an amorphous feature that is most likely related to the loss of $Ga_{(l)}$.

Table 4 - Comparison of Ga:Ge for the samples exposed to a sustained/cycled thermal gradient. Mean at% values for Ga and Ge were determined from three EDX measurements per surface, and then the Ga:Ge ratio calculated.

Sample		Ga:Ge
9_MS_SPScyc	Hot	0.53
	Cold	0.53
10_MS_SPSsus	Hot	0.57
	Cold	0.51

The STEM-EDS data on a dispersion of the metallic protrusion that emerged in the thermal gradient tests are a clear indicator that the sample is extruding Ga (as well as α-Ge). Both sustained and cycled thermal gradients across BGG samples result in destabilization and decomposition of the sample. No evidence of crystalline Ga/Ge oxides were observed in any of the samples. The emergence of supercell reflections after annealing suggests that the evolution of Ga and Ge leads to a range of BGG compositions; *e.g.*, $Ba_8Ga_xGe_{46-x-y}\square_y$ where x<5, as described by Okamoto *et al*. [10]. Therefore, the supercell features seen here are likely to result from the formation of vacancies in the clathrate structure, which arise from the significant loss of Ga/Ge on the 6c position. The crystal structure of $Ba_8Ge_{43}\square_3$, *i.e.*, the supercell structure, was reported by Carillo-Cabrera *et al.* in 2000, which describes that if the Ge(1) position *i.e.*, the 6c Wykoff site, is vacant, then a split site will arise to give Ge(31) and Ge(32) positions [17].

Similarly, the reason why no supercell reflections are observed in the lower temperature annealed samples and on the vacuum annealed sample is because the level of vacancies is not below the threshold value of x = 5. This direct correlation of Ga and Ge loss and the emergence of supercell features resembling the work of Okamoto *et al.* can be related to previous work on the Sn clathrates [20]. The discovery of minute vacancies in the $Ba_8Ga_{16}Sn_{30}$ Type-I clathrate using low temperature neutron and X-ray studies corroborates the concept that the vacancies are forming on the 6c site of the host structure [21]. The difficulty in distinguishing the occupancies of Ga and Ge using X-rays in BGG are likely to have been the reason why this has been overlooked previously in similar clathrate structural studies. Furthermore, superstructure features do not arise until the Ga: Ge ratio is destabilized and a sufficient proportion of vacancies are present, which requires

instrumentation with high signal: noise resolution and a thorough experimentation regime [22].

We can therefore explain some of the unusual property measurement features observed previously. The drop in thermal diffusivity observed by May *et al.* coincides with the temperature at which the Ga and α-Ge are evolved from the samples in this work. It could be that their anomalous results above room temperature are an artefact of the sample decomposition. Returning to the multiple conduction band theory of Kunetzov *et al.*, we can suggest that electron-like, hole-like and mixed electron-hole bands could be present in BGG based on the emergence of vacancies in the structure [23]. Moreover, the valence band of BGG was studied by Tang *et al.*, who showed the presence of three bands using high resolution photoelectron spectroscopy, corresponding to the same hypothesis [24]. Thus, it is clear that the change in BGG clathrate composition as a result of exposure to high temperatures will have an effect on the physical properties of the system, and a deeper assessment of this will be provided in a subsequent article.

Conclusions

This study demonstrates that BGG possesses sluggish decomposition kinetics. The heating environment (air/inert gas/vacuum) has a significant influence on the thermal profile of the clathrate, where heating in vacuum hinders the loss of Ga and α-Ge, but does not prevent it. Meanwhile, an air environment enhances the decomposition, as expected. Surprisingly, no crystalline oxides are evident. The thermal profiles for the annealed samples *versus* the as-prepared clathrate demonstrate that the clathrate melting feature is diminished by exposure to temperatures of 300-730 °C in air and 730 °C in vacuum. By annealing powdered samples, the PXRD data and thermal analysis of the samples reveal that the sample decomposes with the evolution of α-Ge, an unknown phase and an amorphous component. The latter is likely to be a result of Ga melt expulsion from the clathrate. We can unequivocally state that the structural integrity of bulk BGG is not retained upon exposure to sustained or cycled heating regimes in air, where globules of Ga were shown to form on the outer surfaces of the pellets. It is therefore prudent to comment on the fact that previous results showing BGG to be stable at high temperature have not gone far enough to prove that the sample is unaffected during high temperature property measurements. More generally, thorough thermal stability and kinetic studies of samples for thermoelectric materials at high temperature are lacking, and this must be addressed by the thermoelectric research community.

Acknowledgements

The authors gratefully acknowledge funding from the Danish National research Foundation (DNRF93). A.B.B. would like to thank the SINO Danish Center for funding. We would like to thank J. Chevalier for performing the SEM-EDX analysis, Dr. K. Kato and colleagues for assistance with the synchrotron radiation experiments performed at SPring-8, and Jonas Beyer for insightful discussions. We thank the RIKEN-Spring8 center for beam time at beamline BL44B2 (RIKEN proposal no. 20150018 and no. 20160037).

Notes and references

1 M. Christensen, S. Johnsen and B. B. Iversen, *Dalton Trans.*, 2010, **39**, 978.
2 J. D. Bryan, N. P. Blake, H. Metiu, G. D. Stucky, B. B. Iversen, R. D. Poulsen and A. Bentien, *J. Appl. Phys.*, 2002, **92**, 7281.
3 M. Christensen, N. Lock, J. Overgaard and B. B. Iversen, *J Am. Chem. Soc.*, 2006, **128**, 15657.
4 M. Christensen, A. B. Abrahamsen, N. B. Christensen, F. Juranyi, N. H. Andersen, K. Lefmann, J. Andreasson, C. R. H. Bahl and B. B. Iversen, *Nat. Mat.*, 2008, **7**, 811.
5 V. L. Kuznetsov, L. A. Kuznetsova, A. E. Kaliazin and D. M. Rowe, *J. Appl. Phys.*, 2000, **87**, 7871.
6 A. Samarat, G. Svensson, A. E. C. Palmqvist, C. Stiewe, E. Mueller, D. Platzek, S. G. K. Williams, D. M. Rowe, J. D. Bryan and G. D. Stucky, *J. Appl. Phys.*, 2006, **99**, 023708.
7 E. S. Toberer, M. Christiansen, B. B. Iversen and G. J. Snyder, *Phys. Rev. B*, 2008, **77**, 075203.
8 J. Martin, H. Wang and G. Nolas, *Appl. Phys Lett.*, 2008, **92**, 222110.
9 A. May, E. S. Toberer, A. Saramat and G. J. Snyder, *Phys. Rev B*, 2009, **80**, 125205.
10 N. L. Okamoto, K. Kishida, K. Tanaka and H. Inui, *J. Appl. Phys.*, 2006, **100**, 073504.
11 D. Cederkrantz, A. Saramat, G. J. Snyder and A. E. C. Palmqvist, *J. Appl. Phys.*, 2009, **106**, 074509.
12 J. E. Köhler, R. Heijl, L. G. H. Staaf, S. Zenkic, E. Svenman, A. Lindblom, A. E. C. Palmqvist and P. Enoksson, *Smart Mater. Struct*., 2014, **23**, 095042.
13 L. Lutterotti, Nucl. Instrum. Methods Phys. Res., Sect. B, 2010, 268, 334.
14 A. Bentien, E. Nishibori, S. Paschen and B. B. Iversen, Phys. Rev. B, 2005, 71, 144107.
15 B. Essenman, H. Schäfer and R. Zagler, J. Less-Common Metals, 1986, 118, 43.
16 M. Christensen, PhD Dissertation, "*Guest-Host Interactions in Potential Thermoelectric Materials*", 2006, Aarhus Universitet.
17 W. Carrillo-Cabrera, J. Curda, K. Peters, S. Paschen, M. Baenitz, Y, Grun and H. G. von Schnering, Z. Krist. NCS, 215, 2000, 321.
18 W. Carillo-Cabrera, J. Curda, H. G. von Schnering, S. Paschen and Y. Grin, Z. Kristallogr. NCS, 2000, **215**, 207.
19 U. Aydemir, PhD dissertation, "Preparation and Characterization of Clathrates in the Systems Ba-Ge, Ba-Ni-Ge, and Ba-Ni-Si." 2012, Technische Universität Dresden.
20 A. Kaltzoglou, T. Fässler, M. Christensen, S. Johnsen, B. Iversen, I. Presniakov, A. Sobolev and S. Shevelkov, J. Mater. Chem., 2008, **18**, 5630.
21 S. Christensen, M. A. Avila, K. Suekuni, R. Piltz, T. Takabatake and M. Christensen, Dalton Trans., 2013, **42**, 14766.
22 M. Christensen, N. Lock, J. Overgaard and B. B. Iversen, *J. Am. Chem. Soc.*, 2006, **128**, 15657.
23 C. Candolfi, A. Ormeci, U. Aydemir, M. Baitinger, N. Oeschler, Y. Grin and F. Steglich, *Phys. Rev. B*, 2011, **84**, 205118.
24 J. Tang, J. T. Xu, S. Heguri, K. Akai and K. Takigaki, *J. Electronic Mater.*, 2011, **40**, 769.